# Large-field scanning laser ablation system

by F. E. Doany T. Ainsworth

N. Bobroff

D. Goodman

A. E. Rosenbluth

A large-field scanning imaging system has been developed to perform imaging ablation using 308-nm excimer laser light. A 1× Dysonlike lens images a portion of the mask onto a portion of the substrate to be ablated. The lens has a field of 12 mm and a numerical aperture of 0.05, providing a resolution of about 6  $\mu$ m. A mirror system comprising a roof and a plane mirror, with all three surfaces mutually orthogonal, ensures that the mask and the substrate have identical orientations. A common stage is used to hold the mask and the substrate. The stage is scanned in a serpentine manner to transfer the entire image. The illuminated region is diamondshaped, and adjacent scans overlap by half its width to ensure uniformity. Illumination uniformity is provided by a light tunnel in the illumination system. Alignment is performed by optically combining images of mask marks and substrate marks formed by a pair of microscope objectives, one viewing the mask and the other viewing the substrate. The substrate is leveled, focused, and registered relative to the image of the mask by a stage with six degrees of freedom.

# Introduction

The discovery of the laser ablation phenomenon was first reported by R. Srinivasan and V. Mayne-Banton of IBM Research in 1982 [1]. Initial studies by Srinivasan and co-workers [1, 2] showed that pulsed ultraviolet laser radiation at 193 nm can be used to etch organic polymers several micrometers in depth. Additional studies during 1984 and 1985 by Srinivasan and Braren [3] and by J. Brannon et al. [4] at IBM demonstrated that ablation of polymers can also be achieved at other ultraviolet wavelengths, such as 248 and 308 nm. These early discoveries led to extensive research and development activity both inside and outside IBM, and a comprehensive review of this early work was summarized by Srinivasan and Braren in 1989 [5].

The laser ablation process relies on intense ultraviolet radiation, typically available from excimer lasers (193–351 nm). Because most materials, particularly organic polymers, have very strong absorption at these wavelengths, the laser energy is deposited in a shallow surface layer ( $<1 \mu m$ ). When the laser fluence exceeds a threshold value, the poor thermal conductivity of an organic polymer combined with the short laser pulse duration (<50 ns) results in photoablation of the polymer surface layer. A characteristic of the process is that most of the deposited energy is carried off with the ejected material. Since the surrounding area is subjected to little or no thermal damage, patterns can be ablated in polymers with submicron control. Another property of the process is that the threshold for ablation of metals is significantly higher than for polymers. For metals, the high thermal conductivity results in a larger volume of deposited energy, and therefore a higher threshold for ablation. In the case of patterning polymers over a metal,

•Copyright 1997 by International Business Machines Corporation. Copying in printed form for private use is permitted without payment of royalty provided that (1) each reproduction is done without alteration and (2) the Journal reference and IBM copyright notice are included on the first page. The title and abstract, but no other portions, of this paper may be copied or distributed royalty free without further permission by computer-based and other information-service systems. Permission to republish any other portion of this paper must be obtained from the Editor.

0018-8646/97/\$5.00 © 1997 IBM

#### Figure

Schematic representation of the optical and mechanical systems of the Yorktown Scanning Ablation Tool (YSAT). The laser beam is introduced from the left and is directed to the illumination optics on the upper level of the tool, where the beam is homogenized. The uniform-intensity beam is then directed downward to the mask. The projection lens images the mask on the substrate. The mask and the substrate are held together on a common stage which is scanned to transfer the entire image of the mask onto the substrate.

the metal acts as an extremely effective etch stop for the process. Excimer laser ablation of photoresist and polymers soon appeared as a possible application in the microelectronics industry.

Although the requirements and considerations for ablation process and tooling were well defined by 1986 [6], it took an additional four years for ablation technology to mature into a robust manufacturing process.

The first commercial mainframe computer system incorporating laser ablation technology was introduced by IBM in 1991 (the IBM ES/9000® system) [7]. The 308-nm excimer laser ablation process was used to create the vertical interconnections (vias) in the polyimide/copper thin-film redistribution layers of the glass-ceramic multichip modules (MCMs). The evolution of this via ablation technology to the manufacturing level has required comprehensive development of all aspects of this technology, including the ablation process, the mask technology, and the laser tooling. IBM has spent much time and effort to develop the laser via ablation technology and its use in multilevel thin-film packaging. Details of the IBM via ablation process can be found in [8–10].

Laser ablation has proven to be a simple and reliable process for via formation. The four basic steps involved are polymer application, polymer curing, laser ablation, and plasma treatment for debris removal. Typical etch rates for the ablation process are in the range of 0.1-0.3  $\mu$ m per pulse at laser fluence levels of 150-400 mJ/cm<sup>2</sup>. Thus, via formation by laser ablation in polymers  $\sim 10~\mu$ m

thick requires approximately 100 pulses. The critical parameters for laser ablation, the fluence and the number of pulses, can be easily controlled. For industrial excimer lasers providing  $\sim 500$  mJ per pulse, the fluence levels required for ablation dictate an exposure area in the range of 1–2 cm<sup>2</sup>. The 300-Hz repetition rate of these excimer lasers suggests that the laser ablation process can be accomplished in less than 1/2 s for the 2-cm<sup>2</sup> exposed area.

The via ablation system used by IBM in manufacturing is a step-and-repeat projection laser ablation tool very similar to a photolithography stepper. The light source, however, is replaced with a 150-W XeCl excimer laser. Typical MCM substrates may contain about a hundred chip sites, each with several hundred vias. Once a chip site on the substrate is aligned with the mask, the image of the mask is transferred onto the substrate. The laser fluence and number of pulses are adjusted to ablate features directly into the polymer. The several hundred vias within one chip site are ablated simultaneously to open up the underlying metal bonding pads to allow subsequent chip attachment. Once the vias are fully ablated, the substrate is stepped to the next chip site and the ablation process repeated until the entire part is completed. The most recent generation of automated tools in IBM manufacturing process a 127-mm × 127-mm part containing more than 50000 vias in about 12 minutes [10].

These first-generation tools provide a reliable and costeffective manufacturing process for via formation in stepand-repeat applications. That is, the via pattern of a specific individual chip site can be repeated over the entire substrate. The next challenge is to develop a new ablation tool for future high-density multilevel thin-film packages for MCMs. These three-dimensional thin-film wiring levels require ablation of finer features, more tightly registered alignment of features, and, most significantly, ablation of nonrepeating patterns across the substrate. The nonrepeating patterns are required for the specialized level-to-level interconnectivity for each chip site that is needed in the multilevel thin-film package. Using conventional step-and-repeat tools may involve changing masks for every individual chip site on the MCM (potentially more than a hundred masks!). For this application, IBM Research at Yorktown developed the full-field Yorktown Scanning Ablation Tool (YSAT) [11, 12], which uses a projection lens to image a portion of a full-field mask onto a portion of the substrate. The mask and substrate are held together on a common stage that is raster-scanned to transfer the entire mask pattern onto the substrate.

# Full-field scanning ablation system

The approach taken for ablation of vias in a large field is a scanning imaging system with a XeCl 308-nm excimer laser at the source. **Figure 1** shows a schematic of the complete optical system. The system incorporates illumination optics, projection optics, a common scan stage holding the mask and the sample substrate, and alignment optics. Briefly, a 1× Dyson-like lens with a 12mm field images a portion of the mask onto the substrate. A common stage is used to hold together the mask and the substrate, and it is moved in a serpentine manner to transfer the entire image. The stage travel allows for substrates as large as 250 mm × 250 mm. The illuminated region is diamond-shaped, with adjacent scans overlapping by half its width to obtain uniformity in scanning. The illumination system includes a four-sided hollow light tunnel to provide uniform intensity. The system also includes an alignment system based on pairs of microscope objectives that simultaneously view the mask and sample substrate alignment marks. Alignment is performed by optically combining the images of the mask and substrate alignment marks. Focus is also found using the alignment system optics. The substrate is leveled, focused, and registered relative to the mask by a motion system with six degrees of freedom that is mounted on the scanning stage. The various subsystems of the entire scanning ablation tool are described in detail below.

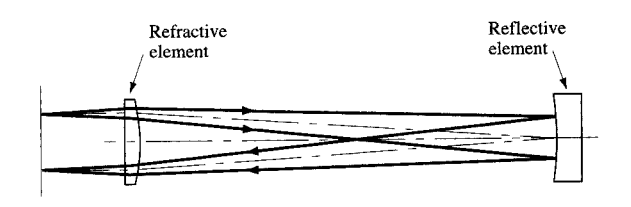
#### • Laser

A XeCl excimer operating at 308 nm, rather than the alternative KrF or ArF excimers, was chosen for several reasons. The ablation rates for polyimide in the 200-400-mJ/cm² region are similar for both 308 and 248 nm (KrF) [4]. In a manufacturing environment, the HCl gas required for XeCl lasers is easier to handle than the  $F_2$  required for KrF lasers. The high-power XeCl industrial excimer lasers are also the most advanced such lasers available on the market. The advanced industrial excimers operating at 308 nm that are available on the market have output powers of  $\geq 150$  W. Typical lasers from XMR Inc.¹ and Lambda Physik GmbH² operate at 300 Hz, producing 500 mJ per pulse. This output level is sustained for more than eight hours of continuous operation.

Because of the high power requirements for an ablation system, the 308-nm wavelength is also more forgiving than deep-ultraviolet radiation for survival of the optics. The high peak powers of the <50-ns pulse widths of the excimer lasers present an additional concern for damage in the optical components. Optical materials and coatings typically have lower absorption and higher damage thresholds at 308 nm than at 248 nm.

## • Projection optics

In comparison to typical photolithographic tools, the excimer laser ablation process involves several constraints.



Schematic representation of the Dyson-type lens. The simple design consists of one refractive element and one reflective

element.

The optical system must accommodate the threshold associated with the ablation phenomenon, the high fluence levels in typical operation, the high laser average power, the very high peak powers associated with the short (<50-ns) laser pulses, and the ultraviolet wavelength. In addition to the susceptibility of optics to damage, the ablation phenomenon requires an optical system with a long working distance because of the debris generated by the process. Furthermore, the optomechanical tolerances are severe as a consequence of the scanning nature of the system.

For optical system survival in a manufacturing environment, the above criteria suggest that only fused silica transmitting elements with low absorption can be used. A minimal path through the transmissive optics must be achieved. The power density within or near individual optical components must be low. Optical coatings must also withstand the high laser peak powers associated with the pulsed excimer lasers, and it is advantageous to avoid edges or corners in the optical system which might be more susceptible to damage. Finally, it is desirable to make the optical components simple and inexpensive in case long-term photodegradation occurs in the manufacturing environment.

A simple scanning system using a common stage dictates the use of a projection lens with magnification of  $+1\times$ . A typical refractive lens is not desirable because of the long glass path length under these high-power applications. For optomechanical stability, a short mask-to-substrate distance is desired—the tolerance required for holding a mask and a substrate on a common stage in a scanning system increases with increasing mask-substrate separation.

A Dyson-type projection lens was found to be optimal for this application. Figure 2 shows the simple design containing one refractive component and one reflective

XMR Inc., 5403 Betsy Ross Drive, Santa Clara, CA 95054.

<sup>&</sup>lt;sup>2</sup>Lambda Physik GmbH, Hans-Boeckler-Strasse 12, W-3400 Gottingen, Germany.

# Figure 3

The Dyson lens with folding mirrors to provide a compact optical system with relatively short mask-to-substrate distance: (a) Image orientation with two folding mirrors (three reflections); (b) correct image orientation using a roof mirror which allows scanning (four reflections).

component. The lens is designed to operate at 308 nm at a numerical aperture (NA) of 0.05 and is achromatic over the laser bandwidth of about 1 nm. The resolution of this lens is therefore 6  $\mu$ m ( $\lambda/NA$ ). The relatively low numerical aperture provides a long depth of focus of  $\pm 60~\mu$ m ( $\lambda/2NA^2$ ). The lens has a field diameter of 12 mm and is doubly telecentric, which ensures its unit magnification performance even at slight defocus conditions. The Dyson-like design in Figure 2 also provides the long working distance required for ablation debris control.

For a scanning system application, two folding mirrors are incorporated in the lens assembly, as shown in **Figure 3**, to provide the compact optical system with a short mask-to-part distance. However, the lens with two simple folding mirrors depicted in Figure 3(a) provides an

inverted image of the mask onto the part  $(-1\times)$ . In order to achieve the  $+1\times$  condition required for scanning, an additional reflection must be provided within the lens assembly. Replacing one of the two folding mirrors with a roof mirror ensures the proper parity. The configuration providing the correct image orientation is shown in Figure 3(b). The roof mirror assembly comprises two mirrors oriented at a right angle to each other intersecting at a line on the edge of the mirrors. To avoid laser damage at this edge, the roof mirror is not straddled by the imageforming beam. Instead, the field of the lens is large enough to allow the image-forming beam to be fully contained within each of the two individual mirrors of the roof mirror assembly.

Although avoiding straddling the roof mirror reduces the tolerances on assembly in terms of the static imaging performance, the scanning nature of the system imposes more stringent tolerances on the overall optical system which dictate the resolution of the tool. As shown in Figure 3(b), the roof mirror and plane mirror are assembled as one unit. As discussed below, the relative positions of the mirror assembly and the lens components are not critical. These positional errors produce a displacement of the image on the substrate, resulting in a constant offset which can be accommodated in the alignment system. Internal angular errors in the prisms have a much greater effect on resolution, and make assembly of the prisms the least routine step in fabricating the optics.

## • Tolerances in prism assembly

Figure 4 is a schematic representation of the four reflections in the YSAT optical path: the three reflections from the mirrored surfaces of the prisms, and the fourth focusing reflection from the primary mirror (with center of curvature at C). In the absence of manufacturing errors, the optics shown in Figure 4 use an even number of reflections to impose a null rotation (i.e., 0° net deviation) on all incident rays. The system therefore has the unusual property that rotation of the entire assembly in three dimensions does not rotate the image; that is, the 0° net deviation is invariant under arbitrary 3D rotation of the optics. (Many prism systems are, of course, insensitive to rotation within a particular 2D plane.) We show below that this constant-deviation property continues to apply when the prism triad is separately rotated or translated relative to the focusing mirror.

The following first-order formula, derived from somewhat lengthy vector-algebraic manipulations, relates the translation and rotation of an image point to the internal errors (translation and rotation) of the prism system:

$$\vec{i} = \vec{o} + 2\vec{i}_{0} + 2(\delta \vec{C}^{(3)} - \delta \vec{R}^{(3)}) + 4\delta \vec{s}_{3} \times \vec{i}_{0} + 2(\delta \vec{s}_{3} - \delta \vec{s}_{r} - \kappa_{12} \delta e_{12} \hat{m}_{3}) \times \vec{o} + O(\delta s^{2}, \delta C^{2}, \delta R^{2}, \delta e^{2}).$$
(1)

Object and image positions in Equation (1) are described as vectors  $\vec{o}$  and  $\vec{i}$ . The first line of the equation describes the nominal image process (no errors in the prism assembly): the second line gives the translational image shift due to prism errors, and the third line the rotational shift. Equation (1) is inclusive in the sense that only prism errors represented in the given terms will produce firstorder image shifts. The origin is placed at the nominal intersection point of the three mirror surfaces (the point where the surfaces would intersect in the absence of fabrication errors). Since the origin is defined in terms of a system with no mirror errors, one can consider the quantities in Equation (1) to be indirectly referenced against the mask and substrate planes. The quantity  $\vec{i}_0$  is defined as the position of the center of the image field when the prisms are free of errors. As discussed further below, this nominal image center is given by

$$\vec{i}_0 = \vec{C}_0^{(3)}.$$
(2)

Vector  $\vec{C}$  is the position of the center of curvature of the  $1\times$  focusing primary. With a spherical or near-spherical primary, any error in positioning the primary relative to the object and image planes is adequately described by changes in  $\vec{C}$ . The 0 subscript on  $\vec{C}$  in Equation (2) denotes the position of the focusing mirror in an error-free system.  $\delta\vec{C}$  denotes the error in positioning the primary, so that

$$\vec{C} \equiv \vec{C}_0 + \delta \vec{C}. \tag{3}$$

Superscripts in parentheses on a vector denote error-free reflection in one of the mirrors.  $\vec{C}_0^{(3)}$  in Equation (2) thus represents the mirror-image position that the primary's center of curvature would take if reflected by mirror 3 (the 45° mirror), were both mirror 3 and the primary positioned without error.

When the prisms are free of internal errors, the second and third lines of Equation (1) are zero; for Equations (1) and (2) to be consistent in this error-free case, we must then have  $\vec{i}_0 = -\vec{o}_0$ , where  $\vec{o}_0$  denotes the center of the object field. Such a relation indeed obtains so long as  $\vec{o}_0$  and  $\vec{i}_0$  are interpreted as the centers of the intrinsic object and image fields of the lens, i.e., as points conjugate with the center of curvature  $\vec{C}_0$  of the focusing mirror. [This also follows from Equation (2).] The position of a given mask point relative to the geometrical field center is  $\vec{o}_0$ . As noted above, the actual illuminated field in the

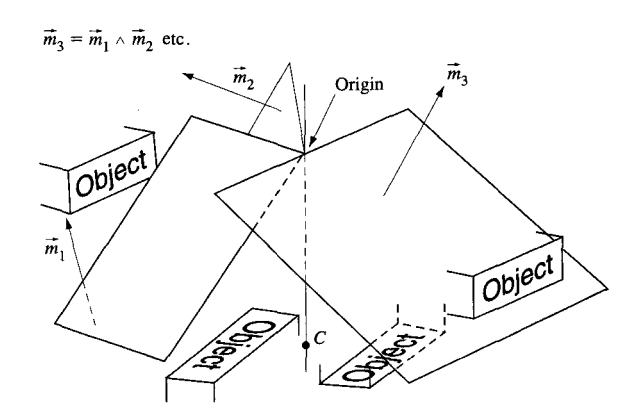


#### Figure 4

Schematic representation of YSAT reflections. An object pattern on the left is first reflected from a roof prism (mirrors 1 and 2), is then reflected by a primary mirror (not shown) with its center of curvature at C, and is finally reflected to the image plane at right by a 45° mirror (mirror 3).

YSAT is offset from the geometrical field center in order that the beam not straddle the roof.

The term  $\delta \vec{s}_3$  in the second line of Equation (1) denotes the rotation error in mirror 3;  $\delta \vec{s}_3$  points along the axis of unintended rotation of this mirror, and has magnitude equal to the rotation angle, assumed small. More formally, if  $\hat{n}_3$  is the surface normal in the prism assembly as fabricated, and  $\hat{m}_3$  the ideal surface normal (i.e., the surface normal obtaining in the absence of fabrication error),  $\delta \vec{s}_3$  specifies the rotation according to

$$\hat{n}_3 \equiv \hat{m}_3 + \delta \vec{s}_3 \times \hat{m}_3. \tag{4}$$

Without loss of generality, Equation (1) assumes that  $\delta \vec{s}_3$  is perpendicular to  $\hat{m}_3$ . In-plane rotation of surface 3 about  $\hat{m}_3$  (its own surface normal) has no effect on the ray reflections, and only components orthogonal to  $\hat{m}_3$  are included in  $\delta \vec{s}_3$ .

The term  $\delta \vec{R}$  is the shift in position of the mirror triad relative to the object and image planes; more precisely, it is the position of the intersection of the three mirror surfaces, defined against an origin at the error-free intersection point. As before, the superscript <sup>(3)</sup> given to  $\delta \vec{R}$  in the second line of Equation (1) denotes reflection in a surface at the position that mirror 3 would occupy in an error-free system.

The term  $\delta \vec{s}_r$  in the third line of Equation (1) specifies the rotation error in positioning the roof prism that is formed by mirrors 1 and 2. In an error-free system, the edge or "spine" of the roof (defined as the line where

$$\hat{\nu}_{12} \equiv \hat{m}_3 + \delta \vec{s}_r \times \hat{m}_3. \tag{5}$$

The first two terms in the third line of Equation (1) thus represent the relative rotation of the roof against the  $45^{\circ}$  mirror. The last term in the third line gives the effect of internal rotation errors in the roof itself: The quantity  $\delta e_{12}$  is the scalar error in the roof internal angle (relative to the nominal 90°). The quantity  $\kappa_{12}$  is defined as +1 for rays that are incident on mirror 1 of the roof before being reflected onward to mirror 2 (see Figure 4), and as -1 for rays that first strike mirror 2 and then mirror 1.

Because of the cross product against  $\vec{o}$ , the third line of Equation (1) represents rotation of the image. [To first order, it is immaterial whether the rotation in this  $1\times$  system is mapped onto the object-space vector  $\vec{o}$ , as in Equation (1), or explicitly onto the image space.] The second line of Equation (1) is independent of object position  $\vec{o}$ , and thus represents a translation error common to the entire image. The error in positioning the mirror triad relative to the focusing mirror,  $\delta \vec{C} - \delta \vec{R}$ , occurs only in the second line, and thus causes image translation but not rotation. Image translation can be corrected with the YSAT alignment system.

Rotations that are first-order can be decomposed into components along orthogonal axes. Rotations about the optical axis cause features to shift within the image plane, while rotations about the two transverse axes introduce focal shifts. The final term in line three of Equation (1), representing error in the roof internal angle, is potentially the most serious rotation contribution. If the incident beam were to intercept the roof edge, roof error would cause rays incident at one side of the edge to be counterrotated against those incident at the other side because of the sign change in  $\kappa_{12}$ . It follows from Equation (1) that the center of this image rotation, mapped into object space, lies at the intersection of the object plane with the axis of rotation,  $\hat{m}_3$ . In YSAT the object and image planes are separated by about 200 mm, so the center of image rotation (for roof internal error) lies about 100 mm from the center of field  $\vec{o}_0$ . The factor of 2 and cross product in Equation (1) imply a rotation in the image that is larger than the roof angle error by a factor of  $\sqrt{2}$ ; moreover,  $\kappa_{12}$ in effect further doubles the image split. If the two parts of the image are allowed to be counter-rotated apart by no more than 1  $\mu$ m, the error in the roof angle must thus be held below about 0.7 arc-seconds, a very stringent angular tolerance.

As noted above, this is one reason for arranging that the input beam not straddle the roof; thus, YSAT was designed with a large enough geometrical field that the actual illuminated field could be fitted entirely on one side

of the roof edge (with all incident rays striking mirror 1 before mirror 2). The roof angular tolerance is thereby improved by much more than 2×, since the static image (i.e., with stage scanning turned off) is no longer split by the rotation. The alignment system then allows the rotation at the center of field to be compensated with a translation. The instantaneous image remains rotated relative to the object, so that blurring does arise when mask and substrate are scanned together, but only in an amount corresponding to the runout in rotation across the width of the illuminated field. (When the leading edge of the scanned illumination field first reaches a given point on the mask, rotation causes its image to be displaced perpendicular to the scan; by the time the trailing edge of the illumination passes over this mask point, its image has rotated to an equal displacement in the opposite direction.) Given a 12-mm illuminated field, the angular tolerance in the roof angle improves to about 12 arcseconds, if, as before, image smear is to be held below 1 μm. Roof error causes a runout in focus that is equally large (since  $\hat{m}_3$  is tilted at 45° to the object and image planes), but in the longitudinal axis such a displacement is negligible, given the 60-µm depth of focus.

Image rotation can also be caused by errors in orienting the roof against the 45° mirror. Equation (1) assumes, without loss of generality, that  $\delta \vec{s}_1$  and  $\delta \vec{s}_2$  are perpendicular to  $\hat{m}_3$ . In general,  $\delta \vec{s}_3 - \delta \vec{s}_r$  has two degrees of freedom within the plane perpendicular to  $\hat{m}_3$ . If  $\delta \vec{s}_3 - \delta \vec{s}_r$  is in the direction parallel to  $\hat{m}_2 - \hat{m}_1$  (see Figure 4), it will also be parallel to the object and image planes, which means that in-plane image rotation will not occur (there will, however, be focus tilt). On the other hand, maximal in-plane rotation occurs when  $\delta \vec{s}_1 - \delta \vec{s}_2$  is parallel to  $\hat{m}_2 + \hat{m}_1$ ; in this case a given angular error in  $\delta \vec{s}_3 - \delta \vec{s}_r$  causes an image smear during scanning of the same magnitude as would be caused were the same angular error present in the roof. Per the discussion above, a tilt between the roof and 45° mirror along this axis exceeding 12 arc-seconds would thus cause the image to be smeared by more than 1  $\mu$ m.

Angular tolerances of this order are well within the range of modern optical shop practice (though the externally oriented configuration of the three mirror surfaces is more difficult than, for example, the inward-facing orthogonal surfaces of the familiar cube-corner). Prototype mirror assemblies with angular errors in the arcsecond range were successfully fabricated at the IBM Yorktown in-house optics shop, and follow-on assemblies of similar quality were procured commercially.

## • Illumination system

The requirements of the illumination system are to accommodate any excimer laser beam shape and divergence, and to produce a uniform intensity

136

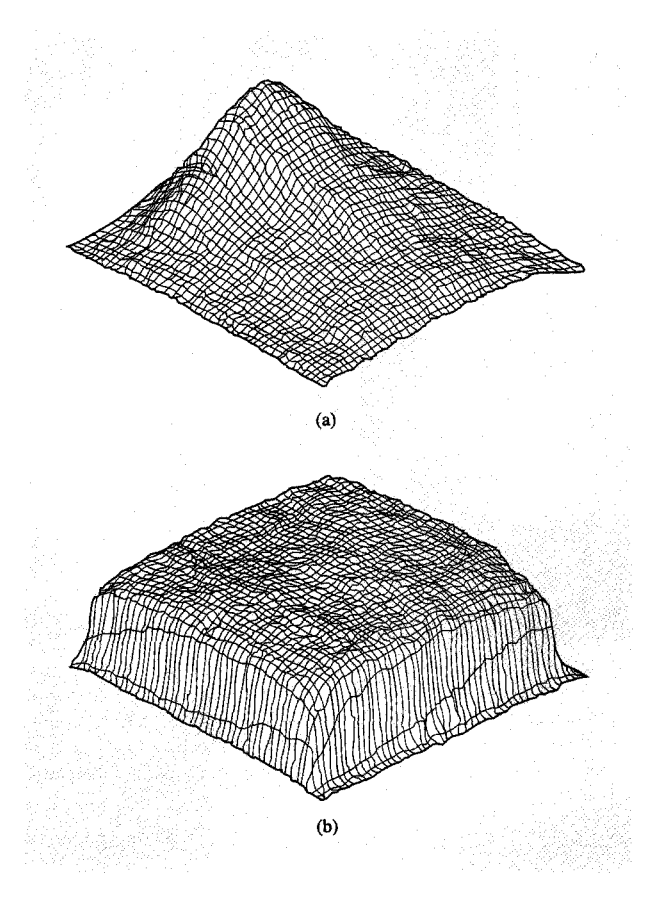
distribution. The laser beam, as produced by the excimer laser, does not provide adequate uniformity for projection ablation. The intensity distribution may also change with time or laser alignment. The laser beam must be homogenized to provide adequate uniformity and to ensure that small changes over time within the input beam distribution are averaged out by the homogenizer.

The homogenizer used is based on the traditional light tunnel, with modifications for high-power lasers. The basic features include a hollow mirror tunnel design, since absorption losses in solid tunnels could be excessive and browning could occur. In addition, the laser beam is focused at the input of the light tunnel, which would eventually cause damage to the input face of a solid light tunnel. The light tunnel mirror coatings are dielectric, especially designed for operation at grazing incidence, to reduce losses and prevent damage to the tunnel substrates. The tunnel itself is held within a cell which is filled with an inert gas. This prevents ionization of the air at the beam focus near the input of the tunnel. The cell also provides a clean environment, preventing the accumulation of dust or other airborne contaminants. At either end, the cell is sealed with planar windows, which are antireflection-coated and placed at a distance from the focus of the beam to prevent damage.

The output of the laser is directed to the light tunnel by two turning mirrors. The turning mirrors also serve to allow alignment of the laser beam into the light tunnel. Since excimer laser beams are typically rectangular in shape, an anamorphic optical relay system [13] is used to produce a square collimated beam. The symmetric collimated beam is then focused into the entrance of the 4-mm  $\times$  4-mm light tunnel at about 0.10 NA. The length of the light tunnel is chosen to ensure a minimum of  $\pm 2$  bounces for the extreme angles of the input beam. This condition produces a uniform intensity distribution at the output plane of the light tunnel.

Proper alignment of the light tunnel results in a square beam with uniformity of  $\pm 5\%$  across the entire output field. Figure 5 shows a three-dimensional beam profile of the input laser beam from a typical excimer laser, as well as the uniform output beam obtained following the light tunnel.

The uniform intensity output of the light tunnel at  $\sim 0.1$  NA is then imaged onto the mask and magnified  $2\times$ , producing an 8-mm  $\times$  8-mm illumination spot at  $\sim 0.05$  NA. These illumination optics also image the light tunnel input into the pupil of the projection lens. Because of the 0,  $\pm 1$ , and  $\pm 2$  bounces in the light tunnel, the image of the source in the pupil is a  $5\times 5$  array of point sources. The 25 point sources (or 49 for  $\pm 3$  bounces) also help redistribute the laser energy and reduce the maximum fluence levels incident on the optical components.



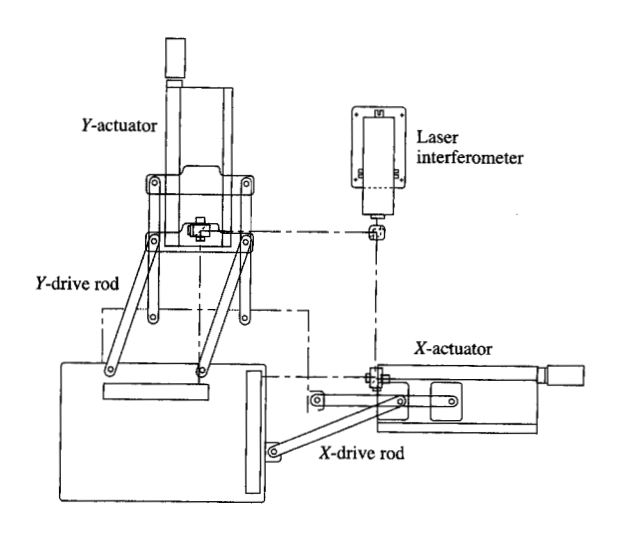
#### 47.1817.184

Laser beam intensity profiles: (a) Intensity distribution of the light produced directly by the laser; (b) uniform distribution produced by the light tunnel homogenizer.

Finally, the light tunnel is oriented at 45° (diamond shape) relative to the scan direction. Scanning with a diamond-shaped field minimizes the errors in exposure on the part. For example, a small offset between successive scans using a square field will result in areas of double exposure or completely unexposed areas. However, in a diamond field scan, successive scans are offset by half the diagonal. Thus, small positional errors produce minimal deviation in exposure doses across the field.

## • Scanning system

The design of the scanning stage is largely constrained by the desired accuracy of image placement. A tilt of the stage causes an inaccuracy in image placement equal to the product of the tilt angle with the vertical separation between the object (mask) and image (substrate) planes. The unit magnification optics were designed to minimize this separation, which scales with the size of the static image field. Since the throughput of the scanner is



#### Floure 6

Schematic representation of the linkage scanning stage system. The stage is attached on the X and Y drive axes to lead screw actuators. A single actuator arm (right) is used on the scan axis, while the orthogonal step axis (top) is attached by drive rods at two points. A plane mirror interferometer is used to precisely determine and control the stage position.

optimized with the largest field allowed by the laser fluence, the large physical size of the optical components produces a relatively large object-to-image spacing. Furthermore, because of the requirement for adequate distance to allow for the removal of ablation debris, the object-to-image spacing could not be reduced to less than 200 mm. To achieve image placement within the specified error of 2  $\mu$ m requires that the maximum pitch or roll of the stage be limited to 10  $\mu$ rad, or about two arc-seconds. This tolerance is especially difficult to achieve, given the 400-mm stroke of the stage. The long travel is necessary to scan substrates 250 mm on a side as well as to reach the substrate load/unload position.

The pitch and roll tolerances are achieved by using a pneumatic bearing stage, which is supported by a polished flat lapped directly on the surface of the granite block which also serves as the tool base. The stage geometry is shown in **Figure 6**. The granite must be flat to 2  $\mu$ m, and the surface is profiled with an electronic autocollimator with 1- $\mu$ rad resolution. It was found that the granite bowed beyond the tolerance within the first year after it arrived from the vendor. After relapping of the surface, no further change has been observed in the following five years. The stage base consists of a rectangular aluminum plate supported at the corners by compensated pneumatic bearings (Fox International, Richmond, CA). The base

plate is machined to reduce weight and increase the mechanical stiffness of the stage assembly. The planar stage design of Figure 6 departs significantly from the usual design of stages supported by pneumatic bearings. Because the stage is guided by an X-Y interferometer system, it was decided that precise physical guideways were not required for the stage. Instead, the stage is attached on the X and Y drive axes to lead screw actuators so that the stage and its drive mechanism are arranged in a plane. This design represents a significant savings in complexity and economy over pneumatic stages utilizing physical guideways and vertically stacked X-Y drive mechanisms. In this case, it also facilitates driving the stage through the center of mass. This is especially important because of the sensitivity of image fidelity to pitch motions induced by the drive system.

A single actuator arm is used on the scan axis, while the orthogonal step axis is attached by drive rods at two points. The two drive rods on the stepping axis limit the yaw motion of the stage to that of the lead screw guideways. Alternatively, three drive stages could be utilized, but this would increase the complexity of the control system and would be an advantage only if active yaw control were desired<sup>3</sup>. The lead screw actuators are linear-motion, zero-backlash lead screw stages supplied by Kensington Inc. The actuators have a 400-mm stroke, and pitch, roll, and yaw are less than 100 μrad. The drives are mounted parallel to the granite flat to 20 µm over the full travel to minimize the torque influence on the scanning stage. The drive arms also very effectively decouple torque influences from the lead screw actuators because they are designed to allow some flexure in the vertical plane. However, it is important to maintain mechanical stiffness in the drive plane because of the long mechanical path between the interferometer sensor and the drive point. The pivot points of the drive rods consist of a hardened pin fitted into a duplex pair of preloaded radial bearings. Preloading the inner bearing races effectively removes radial play in the pivot connection. The mechanical resonance frequency in the drive plane exceeds 40 Hz. Yaw motion of the scan stage is dominated by deviations in the lengths and separations of the drive bars on the stepping axis from a true parallelogram. The matching drive rods and spacers were fabricated together on a mill. The yaw is less than 150  $\mu$ rad for the 0.125-rad pivot required to print a 200-mm substrate.

The lead screw actuators are directly driven by a high-torque motor. The digital error signal is derived from a Hewlett-Packard 5501 plane mirror interferometer using an up/down counter from Excel Precision. Each count represents a stage motion of 80 nm. The stage can slew at

<sup>&</sup>lt;sup>3</sup>R. Kendall, IBM Microelectronics Division, E. Fishkill facility, Hopewell Junction, NY, private communication, 1989.

100 mm/s for rapid unloading of the substrate or mask. The scan speed during printing is determined by the fluence of the excimer laser and the dimension of the scan slit. Typical scan speeds are 10–20 mm/s, with a velocity control of 2%.

## • Alignment and focus system

The task of the alignment and focus system is to orient the substrate precisely with respect to the mask, including duplication of any offset of the projection lens, and to place the substrate in the correct (focal) plane. The system consists of optics, mechanics, and software. The optics allow for simultaneous viewing of alignment marks on both the mask and the substrate, and include an adjustable image shift to match a fixed offset in the projection lens. The mechanics allow for moving the substrate relative to the mask on a six-degree-of-freedom stage for leveling, focus, and alignment. The coupled motion of the alignment stage (six motorized micrometers) is completely under software control.

The alignment/focus system is schematically depicted in Figure 7. The system consists of two pairs of microscope objectives. Each pair views two alignment marks, one on the substrate and the other on the mask, and presents a superimposed image of the mask and substrate marks to the operator on a monitor screen. The images from each pair of microscope objectives are combined in a prism assembly which ensures that correct parity in the mask and substrate images is maintained. A tube lens then relays the superimposed images onto the CCD camera.

Visible light is used for illumination in the alignment system. The infinity-corrected 0.4-NA microscope objectives provide approximately 1.4-\mu resolution. The alignment marks on the substrate are typically under several micrometers of polyimide. These rough metal marks underneath the dielectric layer are viewed using dark-field illumination. Provisions were made to allow both dark-field and bright-field illumination for the mask. The type of illumination can be optimized according to the nature of the mask marks. The illumination is directed to the mask and substrate using fiber illuminators from a remote source. Independent sources are used for the mask and part illuminators to allow independent control of light levels. This minimizes the heat sources in the vicinity of the alignment optics. The upper objective which views the mask is fixed; the lower objective is on an X-Ytranslation stage to provide for matching the offset of the projection lens.

Leveling and focusing of the substrate are also accomplished using the alignment system. Prior to alignment, three points on the substrate are used for focus and leveling. The alignment optics provide a depth of focus of only  $\sim 2~\mu m$ . Since the projection lens has a depth of focus of  $\sim 60~\mu m$ , the leveling procedure using

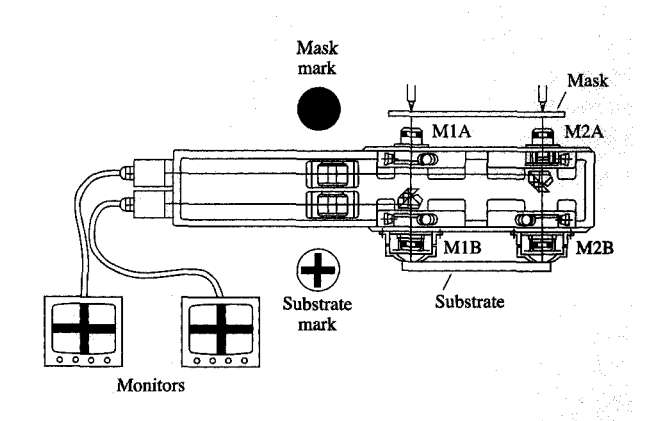


# Figure 7

Schematic representation of the alignment/focus optical system consisting of two pairs of microscope objectives (M1A, M1B; M2A, M2B). Each pair views two alignment marks, one on the mask and the other on the substrate. The superimposed images of the mask and substrate alignment marks are presented to an operator on a monitor screen.

the alignment systems guarantees proper focus for ablation.

The mask is held fixed by the mechanical structure of the alignment system, allowing for a lightweight mask holder. All motion for alignment is incorporated in the six-degree-of-freedom substrate stage.

# • Debris control

A by-product of the laser ablation process is the formation of laser "debris." The material that is ejected by the laser ablation process consists of gaseous by-products, carbon, and polymer fragments. Srinivasan et al. [14] have shown that the macroscopic debris does not appear until more than  $0.5~\mu s$  after the laser pulse is incident on the surface. Since the excimer laser pulsewidths are typically less than 50 ns, the ejected debris does not interfere with the incoming light.

The gaseous material can easily be removed by using a vacuum, but the solid material is of greater concern if left unattended. The solids contribute to greater contamination of the surface and may also interfere with incoming light from subsequent pulses. It is therefore advantageous to remove as much as possible of the ejected debris from the ablation area before the next laser pulse begins. Vacuum alone is typically not strong enough to remove the debris from the large volume above the exposed area. A system consisting of forced gas such as nitrogen or helium combined with an exhaust was devised to minimize the effects of the debris and ensure that the exposure volume is free of debris prior to the arrival of the next laser pulse.

Without debris control, large carbon fragments can be redeposited into an area under exposure. Most redeposited fragments can be ablated by subsequent pulses. However, under certain conditions (laser fluence, particle dimensions, mask defects) some of the fragments may be too large for the laser to remove. Under these circumstances, the carbon cluster will prevent ablation of the polymer layer beneath, which results in a carbonencapsulated "cone" of unablated polymer. However, with the devised forced air and vacuum system, as well as the proper choice of laser fluence and over-etch conditions, such debris concerns can be controlled, and clean vias are easily produced. Some debris will, however, still be present on the adjacent polymer surface. This debris can be removed later with either solvents or an oxygen plasma treatment.

# **Summary**

A large-field scanning excimer ablation system was designed and built that is robust enough for a manufacturing environment. The system was built to provide the IBM Microelectronics Division with the capability to extend its thin-film packaging technology for future high-density multilevel thin-film packages for MCMs. The Yorktown scanning ablation tool (YSAT) is the first system capable of large-field imaging ablation.

The optical system used a  $1 \times$  Dyson-type lens at 0.05 NA, providing 6-μm resolution using the 308-nm XeCl excimer laser. The projection lens incorporates a roof mirror and a plane mirror so that the object and image planes are parallel and their orientations are identical. This lens design and folding mirror arrangement also provides a relatively short mechanical distance from the mask to the sample substrate for optomechanical stability. The mask and the substrate are held together on a common stage, which moves in a serpentine manner to transfer the image of the mask onto the substrate. The stage travels for substrates as large as 250 mm  $\times$  250 mm. The illuminated region is diamond-shaped, and adjacent scans are overlapped by half its width, providing illumination uniformity for the entire large-field substrate. The illumination system incorporates a hollow light tunnel to provide intensity uniformity from the nonuniform excimer laser beam. Scanning further increases uniformity by averaging over the field of the lens in the scan direction.

The YSAT also includes an alignment system based on two pairs of microscope objectives. Each pair views alignment marks on the mask and sample substrate simultaneously and provides an overlaid image of the two marks to an operator. Each mark is independently illuminated to optimize viewing conditions for the operator. The operator can, through software control, align the mask and substrate marks with one another.

The optical transmission of the entire system is approximately 0.65. This throughput was achieved by minimizing the number of components and using efficient dielectric antireflection and high-reflectivity coatings. The YSAT demonstrated ablation of vias down to 8  $\mu$ m over full field for sample substrates up to 166 mm  $\times$  166 mm. The critical factors involved in achieving this resolution over the entire field are the optomechanical tolerances required for the prism assembly and the flatness of travel of the scan stage. These requirements are described in detail above. In addition to the resolution, the overlay registration accuracy provided by the YSAT for these large parts is 1.5  $\mu$ m.

For ablation of vias, there is always a metal pad at the base of the ablated via. The metal pads act as extremely effective etch stops, allowing laser exposure doses of  $1.5 \times -2 \times$  nominal dose. This over-etch condition provides sufficient opening in the vias and provides 100% electrical contact. The etch depth control provided by the process, the laser, and the optical system is approximately 10-15%. A typical etch depth variation of  $\pm 1 \mu m$  has been achieved for ablation depths of about 8 µm. The primary concern is etch depth dependence on feature size. Small features near the optomechanical resolution of  $6-8 \mu m$ may etch at lower rates than larger features. However, for feature dimensions much greater than 8  $\mu$ m (for example,  $\geq$ 15  $\mu$ m), the etch depth produced by ablation is quite uniform. Thus the laser ablation via process, without the wet chemical processing associated with typical photolithographic processes, has been accomplished using the full-field laser ablation system.

## **Acknowledgments**

Numerous individuals at the IBM Thomas J. Watson Research Center and other IBM locations have contributed significantly to the development and implementation of the scanning excimer ablation technology. In particular, the authors wish to acknowledge Jean-Claude Chastang, George Chiu, Steve Lovas, Richard Myer, Rick Rand, Rama Singh, Chris Surovic, and Janusz Wilczynski for their technical contributions to the development of the YSAT.

 $\ensuremath{\mathsf{ES/9000}}$  is a registered trademark of International Business Machines Corporation.

## References

- 1. R. Srinivasan and V. Mayne-Banton, "Self-Developing Photoetching of Poly(ethylene terephthalate) Films by Far-Ultraviolet Excimer Laser Radiation," *Appl. Phys. Lett.* **41**, No. 6, 576–578 (1982).
- R. Srinivasan and W. J. Leigh, "Ablative Photodecomposition: Action of Far-Ultraviolet (193nm) Laser Radiation on Poly(ethylene terephthalate) Films," Appl. Phys. Lett. 104, 6784 (1982).

- R. Srinivasan and B. Braren, "Ablative Photodecomposition of Polymer Films by Pulsed Far-Ultraviolet (193nm) Laser Radiation: Dependence of Etch Depth on Experimental Conditions," J. Polym. Sci. 22, 2601–2609 (1984).
- J. H. Brannon, J. L. Lankard, A. I. Baise, F. Burns, and J. Kaufman, "Excimer Laser Etching of Polyimide," J. Appl. Phys. 58, No. 5, 2036–2048 (1985).
- R. Śrinivasan and B. Braren, "Ultraviolet Laser Ablation of Organic Polymers," Chem. Rev. 89, 1303-1316 (1989).
- J. T. C. Yeh, "Laser Ablation of Polymers," J. Vac. Sci. Technol. A 4, No. 3, 653-658 (1986).
- T. F. Redmond, C. Prasad, and G. A. Walker, "Polyimide Copper Thin Film Redistribution on Glass Ceramic/Copper Multilevel Substrates," *Proc. Electron. Compon. Technol. Conf.* 41, 689–692 (1991).
- T. F. Redmond, J. R. Lankard, J. G. Balz, G. R. Proto, and T. A. Wassick, "The Application of Laser Process Technology to Thin Film Packaging," *IEEE Trans. Components, Hybrids Manuf. Technol.* 16, No. 1, 6–12 (1993).
- 9. J. R. Lankard and G. Wolbold, "Excimer Laser Ablation of Polyimide in a Manufacturing Facility," *Appl. Phys. A* **54**, 355–359 (1992).
- R. S. Patel, T. F. Redmond, C. Tessler, D. Tudryn, and D. Pulaski, "Laser Via Ablation Technology for MCMs Thin Film Packaging—Past, Present, and Future at IBM Microelectronics," Int. J. Microcircuits Electron. Packaging 18, No. 3 (1995).
- T. Ainsworth, N. Bobroff, J.-C. Chastang, F. Doany,
  D. Goodman, I. Lovas, R. Myer, R. Rand, A. Rosenbluth,
  R. Singh, C. Surovic, and J. Wilczynski, "Scanning
  Excimer Ablation Tool," *IBM Tech. Disclosure Bull.* 34,
  No. 7A, 232-233 (1991).
- D. Goodman, T. Ainsworth, N. Bobroff, J.-C. Chastang, F. Doany, I. Lovas, R. Myer, R. Rand, A. Rosenbluth, R. Singh, C. Surovic, R. Tibbets, and J. Wilczynski, "Scanning Excimer Ablation System," presented at OSA Annual Meeting, San Jose, CA, 1991.
- J.-C. Chastang, F. Doany, and D. Goodman, "Anamorphic Afocal Imaging Beam Reshapers," presented at OSA Annual Meeting, 1990.
- R. Srinivasan, K. G. Casey, and B. Braren, "Sub-Nanosecond Probing of the Ablation of Polyimide (Kapton<sup>TM</sup>) by Ultraviolet Laser Pulses," *Chemtron.* 4, No. 3, 153-156 (1989).

Received February 9, 1996; accepted for publication September 7, 1996

Fuad E. Doany IBM Research Division, Thomas J. Watson Research Center, P.O. Box 218, Yorktown Heights, New York 10598 (DOANY at YKTVMV, doany@watson.ibm.com). Dr. Doany is a research staff member in the Optical Systems group at the IBM Thomas J. Watson Research Center. He received a B.S. degree in chemistry from Haverford College in 1978 and a Ph.D. degree in physical chemistry from the University of Pennsylvania in 1984. Dr. Doany was a postdoctoral fellow at the California Institute of Technology from 1984 to 1985, working on ultrafast laser spectroscopy. He subsequently joined IBM at the Watson Research Center, where he worked on laser spectroscopy, laser material processing, and applied optics. Dr. Doany has written many technical papers, holds ten patents, and has received two Research Division Awards from IBM, in 1994 and 1996. He is a member of the Optical Society of America and the Society for Information Display.

Thomas Ainsworth Mr. Ainsworth is a retired research staff member who worked at the IBM Thomas J. Watson Research Center. He was responsible for the design and fabrication of the laser ablation transport and handling systems. Mr. Ainsworth was an early contributor to laser technology in the manufacturing equipment at the IBM circuit packaging facility in Endicott, New York.

Norman Bobroff IBM Research Division, Thomas J. Watson Research Center, 30 Saw Mill River Road, Hawthorne, New York 10532 (BOBROFF at YKTVMV, bobroff@watson.ibm.com). Dr. Bobroff has been a research staff member in computer science at the IBM Thomas J. Watson Research Center since 1993. His current interest is operating systems and serving multimedia files over local area networks. Prior to joining the field of computer science, Dr. Bobroff was involved in optical system testing. He has constructed instruments for the quantitative evaluation of lens performance, and has participated in the development of optical alignment systems for X-ray and optical lithography. He has also been interested in scanning and alignment stages for lithography applications. Prior to joining IBM in 1982, Dr. Bobroff developed a spectrometer to observe stellar radiation at extreme ultraviolet wavelengths from a sounding rocket. He received an S.B. degree from the University of Chicago and a Ph.D degree in physics from the California Institute of Technology in 1983.

Douglas Goodman Polaroid Corporation, Optical Engineering Department, 38 Henry Street, Cambridge, Massachusetts 02139. Dr. Goodman received a B.S. degree in physics in 1969 from Rhodes College, an M.S. degree in 1970 from the University of Illinois, Champagne–Urbana, and a Ph.D. degree in optics from the University of Arizona in 1979. He was a research staff member at the IBM Thomas J. Watson Research Center from 1979 to 1993, when he joined Polaroid Corporation as a senior technical manager. He is a fellow of the Optical Society of America, and has worked in a variety of areas in applied optics, including photolithography, alignment, illumination, optical inspection, microscopy, and metrology.

Alan E. Rosenbluth IBM Research Division, Thomas J. Watson Research Center, P.O. Box 218, Yorktown Heights, New York 10598 (AER at YKTVMV). Dr. Rosenbluth received the Ph.D. degree in optics from the University of Rochester in 1982 as a Hertz Foundation fellow. He has been a staff member at the IBM Thomas J. Watson Research Center since 1982. His principal research activities have been in photolithographic instrumentation and processing, display technology, and thin-film optics.